

# Naval Structural Antenna Systems for Broadband HF Communications

G. Marrocco, *Member IEEE*, and L. Mattioni

**Abstract**—This paper introduces the concept of multipurpose structural antenna system for shipborne installations. By combining properly shaped and loaded wire radiators together with an existing naval superstructure, such as the funnel or a big mast, it is possible to achieve a broadband high-frequency compact radiating system which permits handling both sea-wave and near vertical incidence sky-wave communications. When provided with a plurality of feeding points, the naval structural antenna may be used in multichannel mode, with a huge efficiency improvement over the conventional multichannel broadband systems requiring a combining network. Additionally it is shown that, when fed in monochannel mode, the structural antenna system exhibits focusing features with the possibility to achieve sectorial coverages. This paper demonstrates the advantage and limitation of this new system by carefully taking into account the interantenna coupling.

**Index Terms**—Broadband antennas, high-frequency antennas, loaded antennas, naval communications, software defined radio, structural antenna.

## I. INTRODUCTION

RECENTLY manufactured ships for both civil and tactical purposes are equipped with the Software Defined Radio system [1] having the capability to simultaneously receive and transmit multiple waveforms, of the same or different type, within the 2 MHz–2 GHz frequency range. To host *multi-channel* communications, actual naval systems employ either a small set of broadband antennas together with combining networks or a plurality of narrow-band antennas operating in different subbands. In the first case, because of the losses introduced by the power combiners, the resulting system efficiency can be highly reduced. In the other case, the coexistence of several radiators requires large space and produces undesired interactions among antennas and the ship superstructure. These issues are particularly critical in the high-frequency (HF) range because of the large wavelengths involved.

The problem of efficient antenna installation in the available space has been already considered in the context of avionic environments where, since the late 1950s, some structural solutions have been proposed. In particular, the whole aircraft or some parts of it can be used as radiating element in the HF range, when properly fed (notch or towel bar antennas), since the aircraft size is comparable with the radiated wavelength [2]–[5].

Presently, structural antennas in the naval environment are not so common, although the strong interaction between naval

superstructures and shipborne antennas has been widely argued in past and recent papers. For instance, the suitable integration of typical HF antennas into the ship's topside structure has been discussed in [6] and optimum performances are achieved by the simultaneous design of antennas and naval structures with the aid of scale brass models. Radiation pattern distortions of simple HF antennas, when embedded into the naval scenario, have been considered in [7]. Investigation in [8] addressed the possibility to place an HF or a very high-frequency (VHF) array on the deck, hull, and/or gunwale of a ship with the purpose of sectorial coverage.

This paper focuses on the possibility to obtain a naval structural antenna as integration of one or more wire broadband radiating elements together with an existing metallic structure such as a funnel or a big mast which are rather common in many ship scenarios. The funnel in particular has typically cylindrical, pyramidal, as well as conical shape, and diameter (5–10 m) and height (10–25 m) comparable with HF wavelength. Such a structure is therefore a good candidate to host antennas or even to become part of a radiating system.

The integration that is proposed here, potentially yields a broadband structural antenna system for HF naval communication having the possibility to be driven by one or multiple sources and to communicate at different elevation angles depending on the frequency used and on the particular service to be carried out.

A structural solution also offers the advantages of limited space requirements and the intrinsic compensation of the pattern distortion due to the presence of the naval environment, which is instead partly embedded into the antenna system.

The proposed study will leave apart from a particular naval realization and will consider a canonical test-case with the purpose of investigating the feasibility and potential of the naval structural antenna concept.

This paper is organized as follows. Section II introduces the basic idea of obtaining an HF antenna from a funnel-like structure. The design and performances of a single-feed *naval structural antenna* (NSA) are described in Section III, while the extension to multiple-feed configurations is presented in Section IV. The structural solution is further experimented with in Section V by using different shapes and size of the superstructure. The relevant results are summarized in the final section.

## II. THE RATIONALE OF THE NAVAL STRUCTURAL ANTENNA

Starting from a standard folded monopole antenna, which has been already considered as HF radiator in [9], a basic idea to obtain a structural antenna from a naval funnel consists in replacing one of the vertical conductors of the antenna with

Manuscript received June 28, 2005; revised November 16, 2005. This work was supported by Selex Communications, Finmeccanica Group.

The authors are with Dipartimento di Informatica, Sistemi e Produzione, University of Roma Tor Vergata, Rome, Italy (e-mail: marrocco@disp.uniroma2.it).  
Digital Object Identifier 10.1109/TAP.2006.872559

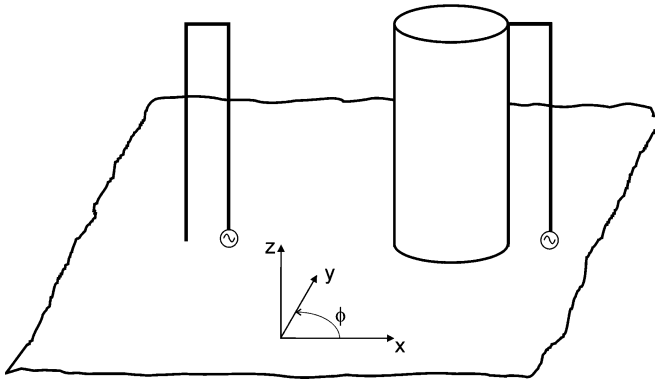


Fig. 1. Basic idea to obtain a structural antenna from a folded monopole-like structure and a funnel-like cylindrical body.

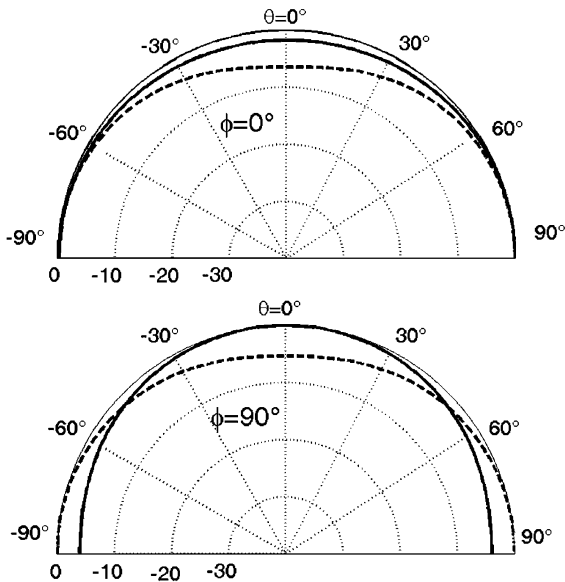


Fig. 2. Normalized directivity at 2 MHz of the folded monopole (dashed lines) of size  $2\text{ m} \times 10\text{ m}$  and of the structural antenna (solid lines) in Fig. 1, including a hollow cylinder with size  $5\text{ m} \times 10\text{ m}$ .

the funnel itself (Fig. 1). The resulting structure recalls the towel-bar antenna feeding technique for the aircraft's fuselage [5].

To illustrate the concept, Fig. 2 shows the normalized gain of a folded monopole of size  $2\text{ m} \times 10\text{ m}$  and its combination with a hollow cylindrical body of height  $10\text{ m}$  and diameter  $5\text{ m}$ . Results have been obtained by means of the method of moments [10], where the cylindrical body has been modeled as an aluminum wire grid and both the systems have been considered on an infinite perfect ground plane, as in all the following simulations. The  $2\text{ MHz}$  patterns are quite similar: in particular, the cylinder-wire antenna shows a nearly hemispherical coverage. Moreover, the uniformity in the directivity at high elevation angles, as well as along the horizon, makes this configuration rather attractive as a multifunction antenna in the sense that it combines the possibility to simultaneously provide sea-wave and near vertical-incidence sky-wave (NVIS at frequency  $2\text{--}7\text{ MHz}$ ) radiation.

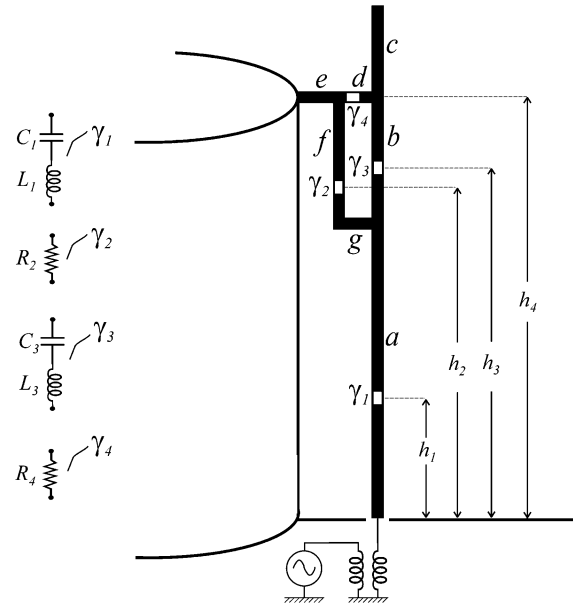


Fig. 3. Example of structural antenna (single-feed NSA) with a shaped *wire subradiator*. Segment size (in [m]):  $a = 7, b = 3, c = 2, d = 1, e = 1, f = 3, g = 1$ . The RF source is connected to the antenna by means of an impedance transformer with step-up ratio  $n = 4$ . Geometrical (in [m]) and electrical parameters of the circuits  $\gamma_n$  are  $h_1 = 3.25, h_2 = 7.75, h_3 = 8.25, h_4 = 10, C_1 = 569.1\text{ pF}, L_1 = 1.12\text{ }\mu\text{H}, R_2 = 61\text{ }\Omega, C_3 = 59.8\text{ pF}, L_3 = 0.073\text{ }\mu\text{H}, R_4 = 48.6\text{ }\Omega$ .

### III. SINGLE-FEED NSA

The above basic structural antenna does not possess broadband features, as required to serve the whole HF range, even if the wires were loaded by lumped or distributed impedances. In recent papers [11], [12], the authors have proposed a new loaded wire antenna for multimode HF broadband communications. This antenna, denoted as *bifolde*d monopole, was derived from the more conventional folded monopole when the basic shape is modified with additional vertical and horizontal wire segments in order to allow a plurality of current paths. In particular, this antenna produces the radiation of a half loop, for NVIS links, and of a monopole for both sea-wave and beyond line of sight communications. The wire part of the structure in Fig. 1, hereafter denoted as *wire subradiator*, has been therefore modified by adding more vertical and horizontal wires. An interesting geometry, among the various considered, is presented in Fig. 3. This shape is conceptually similar to the bifolde

monopole in the sense that it embodies nested closed-loop paths, with the difference that the vertical conductor corresponding to the cylindrical body can not be loaded with lumped impedances. Hence, in order to obtain nested loops also in this geometry, the additional wires are connected only to the principal wires of the folded monopole rather than to the cylindrical body. Finally, the vertical conductor up above the cylinder will be useful to enhance the radiation in the highest part of the HF range, as shown later on.

To achieve broadband features and a radiation pattern suitable to the different kinds of services, the *wire subradiator* has been loaded with lumped impedances chosen as isolated resistors as well as parallel or series inductor-capacitor circuits. An

impedance transformer of step-up ratio to be optimized is connected between the wire-radiator and the radio-frequency (RF) source generator. The inclusion of lumped impedances on the wires plays the double role of matching network and radiation pattern synthesizer. The parameters of such impedances, subjected to the limitations  $50 \text{ nH} \leq L \leq 3 \mu\text{H}$ ,  $5 \text{ pF} \leq C \leq 1 \text{ nF}$ , and  $R \leq 100 \Omega$ , are chosen by a genetic algorithm (GA) optimizer [13] to minimize the following penalty function:

$$F = \frac{1}{N_f} \sum_{n=1}^{N_f} \left[ w_1^{(n)} F_{\text{VSWR}}^{(n)} + w_2^{(n)} F_{\eta}^{(n)} + w_3^{(n)} F_G^{(n)} \right] \quad (1)$$

where  $N_f$  is the total number of frequency samples in the HF range (tagged by index  $n$ ).  $F_{\text{VSWR}}^{(n)}$ ,  $F_{\eta}^{(n)}$ , and  $F_G^{(n)}$  are threshold functions shown in (2)–(4), respectively, controlling the matching, the system efficiency, and the system gain at different elevation angles. Parameters  $\{w_j^{(n)}\}$  selectively weigh these functions in different parts of the band. Reasonable requirements for the conventional loaded antenna systems are  $\text{VSWR} < 3$  within the whole HF range, antenna efficiency larger than 5–10% at lower frequencies (2 MHz–7 MHz) and larger than 50% above 15 MHz, gain higher than  $-20 \text{ dB}$  at NVIS, higher than  $-10 \text{ dB}$  along the horizon for  $2 \text{ MHz} \leq f \leq 5 \text{ MHz}$ , and higher than  $0 \text{ dB}$  above 5 MHz

$$F_{\text{VSWR}}^{(n)} = \begin{cases} 0, & \text{if } \text{VSWR}^{(n)} < s_0^{(n)} \\ \frac{\text{VSWR}^{(n)} - s_0^{(n)}}{\text{VSWR}^{(n)}}, & \text{otherwise} \end{cases} \quad (2)$$

$$F_{\eta}^{(n)} = \begin{cases} 0, & \text{if } \eta^{(n)} > \eta_0^{(n)} \\ \frac{\eta_0^{(n)} - \eta^{(n)}}{\eta_0^{(n)}}, & \text{otherwise} \end{cases} \quad (3)$$

$$F_G^{(n)} = \begin{cases} 0, & \text{if } G^{(n)}(\theta) > G_0^{(n)} \\ \frac{G_0^{(n)} - G^{(n)}(\theta)}{G_0^{(n)}}, & \text{otherwise.} \end{cases} \quad (4)$$

Generally,  $s_0^{(n)}$ ,  $\eta_0^{(n)}$ , and  $G_0^{(n)}$  are frequency-dependent thresholds whose values depend on the system requirements.  $G^{(n)}(\theta)$  controls the system gain at different elevation angles depending on the operating frequency. In particular, system gain has been optimized at the zenith for low frequencies to permit NVIS links and toward the horizon as frequency increases

$$G^{(n)}(\theta) = \begin{cases} G^{(n)}(0^\circ) & 2 \leq f < 7 \text{ (MHz)} \\ G^{(n)}(45^\circ) & 7 \leq f < 11 \text{ (MHz)} \\ G^{(n)}(90^\circ) & 11 \leq f < 30 \text{ (MHz)}. \end{cases} \quad (5)$$

GA is applied together with the method of moments and the evaluation of each population member's (e.g., the loaded structural antenna) features is obtained by the fast method described in [14], which requires the inversion of small matrices, of size only depending on the number of impedances employed. For what concerns the accuracy of the MoM analysis for this class of structures, the authors previously reported in [11] a comparison of simulated VSWR with measurements on a 1:50 scaled model of a broadband HF loaded wire antenna having the same features of the NSA's subradiators. The agreement was rather nice, even at low frequencies.

An example of optimized structure requires four loading impedances as in Fig. 3 and the resulting antenna is well matched

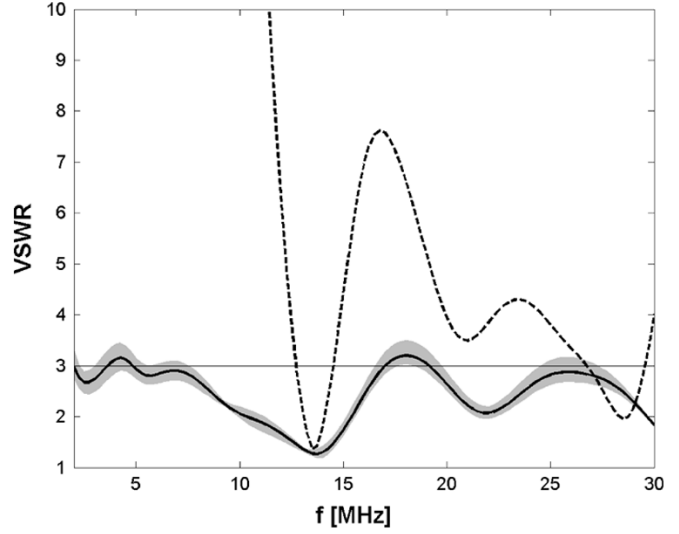


Fig. 4. VSWR for the single-feed NSA of Fig. 3 without (dashed line) and with (solid line) optimized broadbanding loads. The shadowed region gives the sensitivity of the VSWR to a random  $\pm 10\%$  deviation of the electric components values from the optimized results. VSWR curves refer to  $50\Omega$ .

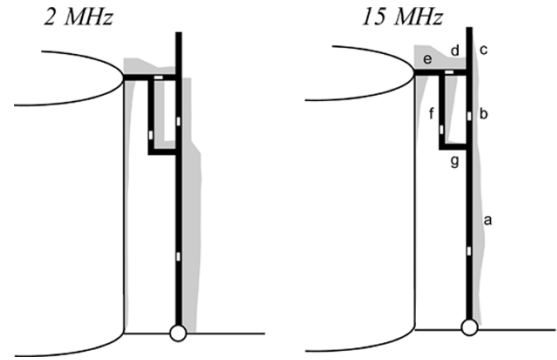


Fig. 5. Currents on the single-feed loaded NSA. Shadowed regions indicate the current amplitude at wire location.

( $\text{VSWR} < 3$ ) in the whole HF range as visible in Fig. 4. The shadowed region gives the sensitivity of the VSWR to a random  $\pm 10\%$  deviation of the electric components values from the optimized results. As expected from the GA paradigm, the optimized antenna appears rather robust to fabrication uncertainties.

The inspection of the antenna current in Fig. 5 reveals the presence, at lower frequencies (2 MHz), of two nested rectangular loops. The smaller one consists of the  $b, d, f, g$  segments and mainly radiates toward the zenith. The external loop acts as a folded monopole of segments  $a, b, d, e$  together with the cylindrical body, with main radiation toward the horizon. The resulting radiation pattern (Fig. 6) still retains hemispherical coverage. As frequency increases (15 MHz) the current pattern becomes more complex, the internal loop mode vanishes, the segment  $c$  starts to be energized, and the radiation is similar to that of a whip antenna, e.g., with nearly omnidirectional pattern on the horizontal plane without the presence of nulls.

The frequency-dependent  $\phi$ -averaged gain at horizon (Fig. 7) reaches  $0 \text{ dB}$  at 5 MHz with peak values of about  $5 \text{ dB}$  beyond 15 MHz. A reasonably high gain also can be appreciated in the NVIS frequency range. Finally, except for 2 MHz, where the

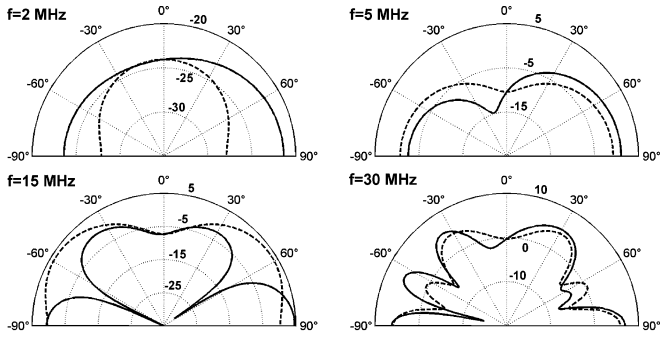


Fig. 6. Gain of the single-feed loaded NSA at some frequencies. Solid line:  $\phi = 0^\circ$ ; dashed line:  $\phi = 90^\circ$ . The wire subradiator is assumed to be placed in  $\phi = 0^\circ$  as in Fig. 1.

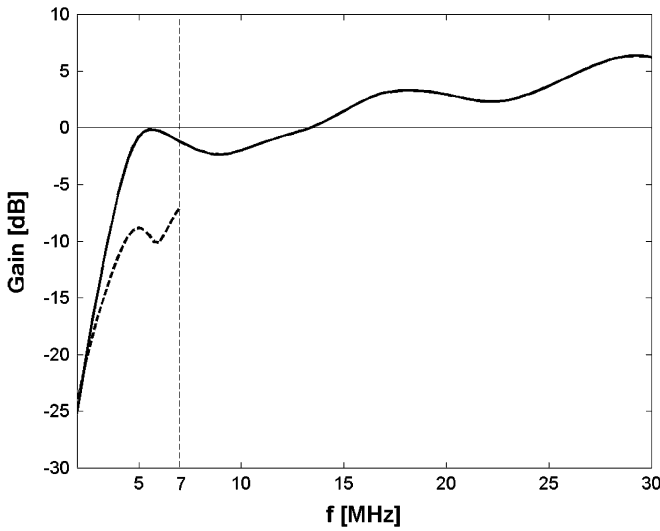


Fig. 7.  $\phi$ -averaged frequency-dependent gain for the single-feed loaded NSA along the horizon ( $\theta = 90^\circ$ , solid line) and at NVIS ( $\theta = 20^\circ$ , dashed line).

efficiency is between 0.2% and 0.5%, acceptable values are obtained in the whole HF range, and in particular beyond 5 MHz, where the efficiency ranges between 30% and 80% (Fig. 8).

#### IV. MULTIPLE-FEED NSA

The inclusion of more than a single wire subradiator on the cylindrical body yields a multiple-feed structure which can be used both in *multichannel* and in *monochannel* configuration, as shown next. Hereafter,  $\text{NSA}_N$  denotes an antenna system with  $N$  subradiators.

As an example, Fig. 9 shows the  $\text{NSA}_4$  configuration including four equispaced wire subradiators. Since wires are placed at a close proximity compared with the HF wavelengths, the mutual coupling effects need to be carefully taken into account in the system performance evaluation, not only for what concerns the radiation properties but also for the electrical mismatch at each port.

##### A. Multichannel Mode

The multichannel feeding strategy allows the antenna to simultaneously communicate on multiple channels. Each port of the structure can be directly excited by a different narrow-band

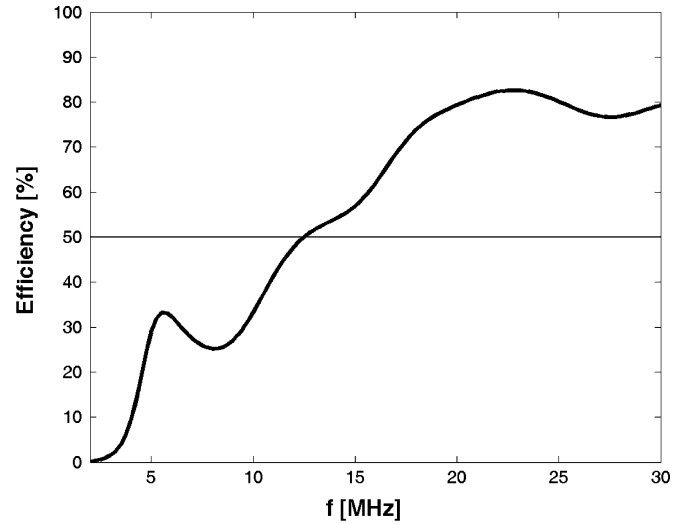


Fig. 8. Efficiency of the single-feed loaded NSA ( $\eta_{\text{NSA}_1}$ ).

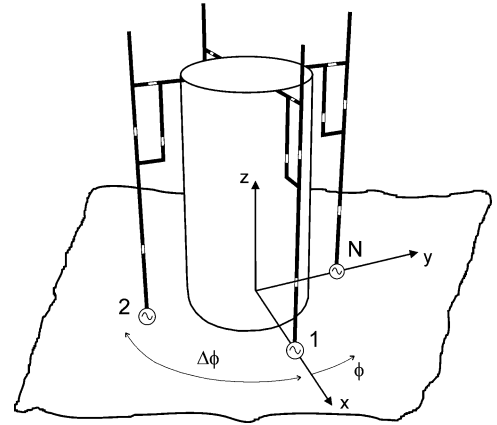


Fig. 9. Multiple-feed  $\text{NSA}_4$ . The four wire subradiators are clockwise numbered.

signal avoiding the use of combining networks that are generally adopted together with traditional broadband radiators. While the efficiency of the single-feed antenna ( $\text{NSA}_1$ ) plus the combiner network with  $N = 2^p$  channels is  $\eta_{A+C} = 2^{-p}\eta_{\text{NSA}_1}$ , the exclusive allocation of each subradiator of the  $\text{NSA}_N$  to a single channel is expected to ideally give a higher system efficiency close to  $\eta_{\text{NSA}_1}$ . However, because of the coupling among subradiators, the *active* efficiency of the  $\text{NSA}_N$  is slightly smaller than  $\eta_{\text{NSA}_1}$ , as shown in Fig. 10 for the case  $N = 4$ . Anyway, it can be appreciated up to 400% improvement in the most part of the band with respect to the  $\text{NSA}_1$  plus the power combiner network. At those frequencies where the port coupling is more effective, the above improvement is smaller but always larger than about 300%.

The *embedded VSWR*, the *active gain*, and the *active efficiency*, e.g., input and radiation characteristics for the multiple-feed NSA when a single source is active while the remaining are turned off and terminated to the line-impedance, have been numerically computed and can be compared with those of the  $\text{NSA}_1$  in Fig. 3. Fig. 11 shows the embedded VSWR for  $N = \{4, 6\}$  equispaced elements. In both the configurations, the mutual coupling among wire subradiators is not so strong to

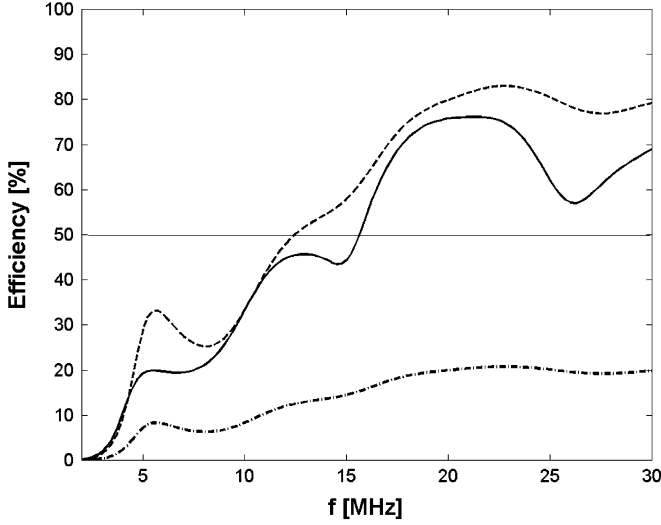


Fig. 10. System (active) efficiency of the NSA<sub>4</sub> in *multichannel* mode (solid line), of the NSA<sub>1</sub> with a single-channel (dashed line), and of the NSA<sub>1</sub> connected to a power combiner for a simultaneous four-channel communication (dash-dotted line).

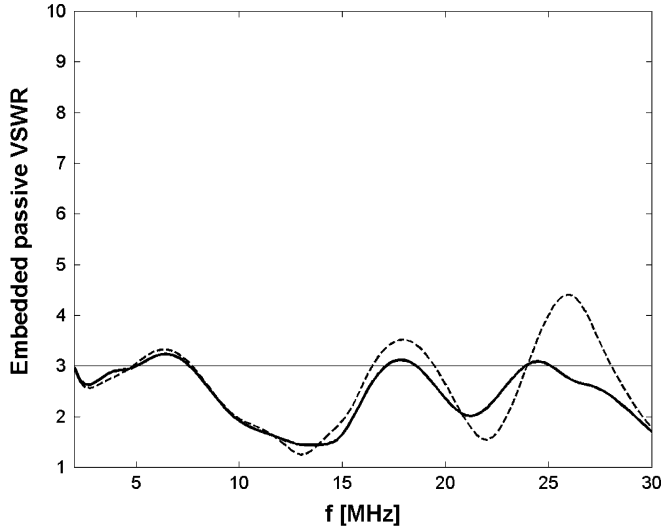


Fig. 11. *Embedded* VSWR of the NSA<sub>4</sub> (solid line) and NSA<sub>6</sub> (dashed line).

sensibly modify the antenna matching in comparison with the single-feed loaded NSA (see Fig. 4).

Figs. 12 and 13 represent the active gain at different frequencies on both horizontal and vertical cuts for the NSA<sub>4</sub>. The azimuthal patterns, particularly at higher frequencies, retain omnidirectional features as in the NSA<sub>1</sub>, and NVIS links are still possible due to the acceptable radiation close to the zenith at lower frequencies.

NSA<sub>N</sub> with  $N \leq 6$  subradiators therefore can be used in multichannel configuration maintaining about the same input and radiation characteristics of the single-feed NSA. For a larger number of elements, the distance between contiguous subradiators reduces and the mutual coupling effects have been verified to degrade the antenna matching.

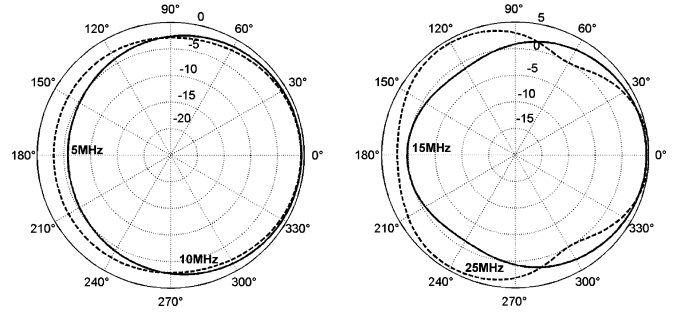


Fig. 12. *Active* gain of the NSA<sub>4</sub> at different frequencies on the horizontal cut ( $\theta = 90^\circ$  plane). The source is assumed to be placed in  $\phi = 0^\circ$ .

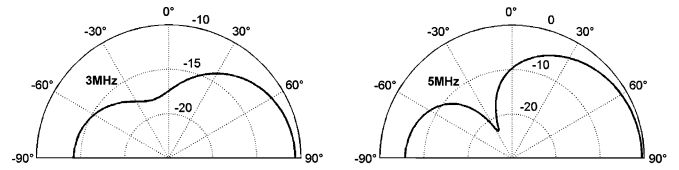


Fig. 13. *Active* gain of the NSA<sub>4</sub> at different frequencies on the vertical cut ( $\phi = 0^\circ$  plane). The source is assumed to be placed in  $\theta = 90^\circ$ .

### B. Monochannel Mode

In the monochannel feeding strategy, the  $N$  ports are simultaneously allocated to the same channel as in array configurations. The following investigation will address the sectorial coverage properties of the NSA<sub>N</sub> that can be achieved by a simple phase synthesis and will analyze the degradation of the system broadband features in comparison with the single-feed antenna (see Fig. 4). Although the overall structure is not properly an array, since there is a tight electrical contiguity among all the radiating elements, nevertheless the system can be considered as a single antenna equipped with  $N$  ports having the possibility to host different current patterns depending on the particular feeding strategy. An active element pattern  $\mathbf{f}_n(\theta, \phi)$  can be associated to each port. Due to the rotational periodicity of the structure ( $\mathbf{f}_n(\theta, \phi) = \mathbf{f}_1(\theta, \phi + (n-1)\Delta\phi)$ ), the total field radiated by the NSA<sub>N</sub> when each port is excited by a current  $I_n = C_n e^{j\alpha_n}$  can be written [15] as

$$\mathbf{E}(r, \theta, \phi) = \frac{e^{-jkr}}{4\pi r} \sum_{n=1}^N C_n e^{j\alpha_n} \mathbf{f}_1(\theta, \phi + (n-1)\Delta\phi) \quad (6)$$

with  $\Delta\phi = 2\pi/N$ . It is easy to observe that beam steering on the horizontal plane at  $\phi_0$  direction can be simply achieved, choosing  $C_n = C_0$ , and

$$\alpha_n = -\mathcal{L}\mathbf{f}_1(\phi_0 + (n-1)\Delta\phi) \quad (7)$$

where “ $\mathcal{L}$ ” denotes the phase operator.

Figs. 14 and 15 show the gain of the NSA<sub>N</sub> on the horizontal plane at different frequencies, respectively, for the cases  $N = 4$ , with beam steering in  $\phi_0 = 45^\circ$ , and for the case  $N = 6$ ,  $\phi_0 = 30^\circ$ . Azimuthal patterns, which are symmetric as regards  $\phi_0$ , have been compared with those of the NSA<sub>1</sub> rotated of  $\phi_0$ . As visible in Fig. 14, at 2 and 10 MHz, the NSA<sub>4</sub> exhibits sectorial coverage capabilities and the radiation is principally confined in the half-space centered on  $\phi_0$  with a front-to-back ratio of about

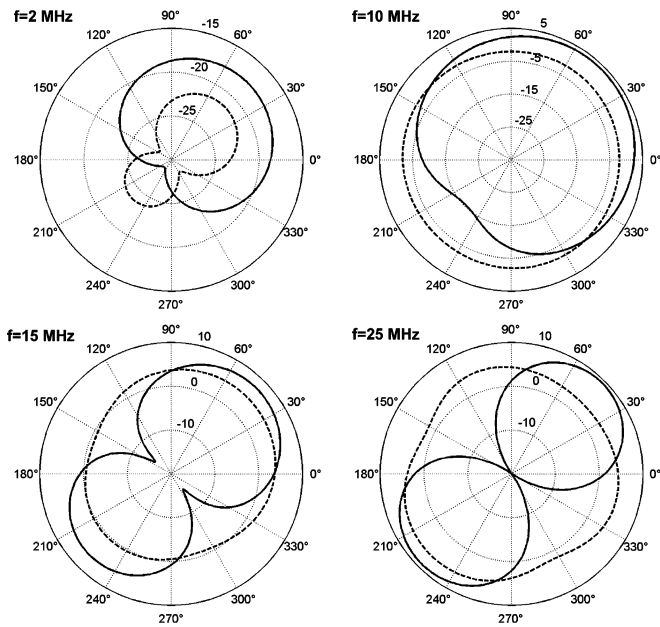


Fig. 14. Azimuthal gain patterns of NSA<sub>4</sub> steered to  $\phi_0 = 45^\circ$  (solid line) compared with those of NSA<sub>1</sub> (dashed lines).

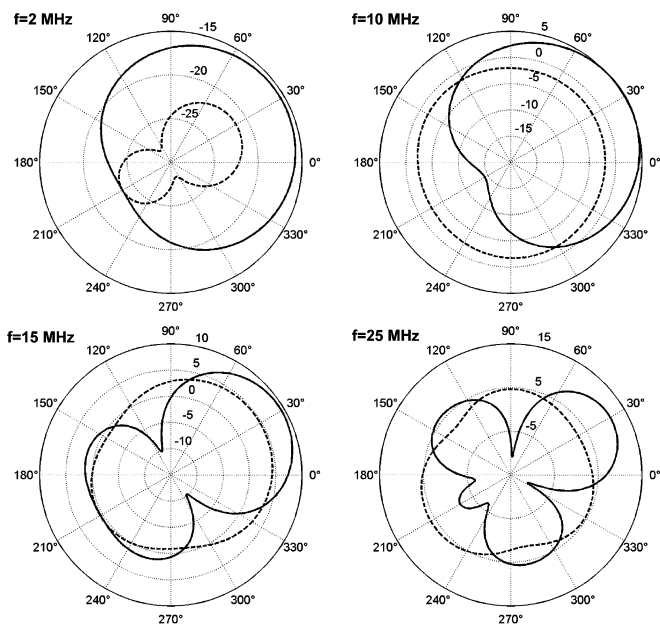


Fig. 15. Azimuthal gain patterns of NSA<sub>6</sub> steered to  $\phi_0 = 30^\circ$  (solid line) compared with those of NSA<sub>1</sub> (dashed lines).

10 dB. Moreover, it can be also observed an improvement on the maximum gain performance of about 5–6 dB with respect to the NSA<sub>1</sub>. As the frequency increases, the front-to-back ratio of the NSA<sub>4</sub> tends to reduce but this configuration still presents a better gain than the single-feed structure along  $\phi_0$ . Using  $N = 6$  subradiators (Fig. 15), a further improvement on the maximum gain performance at all HF frequencies (about 9 dB at 25 MHz) and a better front-to-back ratio at 15 and 25 MHz as regards the NSA<sub>4</sub> can be noted.

Antenna matching can be still considered acceptable for NSA<sub>4</sub> (Fig. 16), while some “blind subbands” appear for NSA<sub>6</sub>

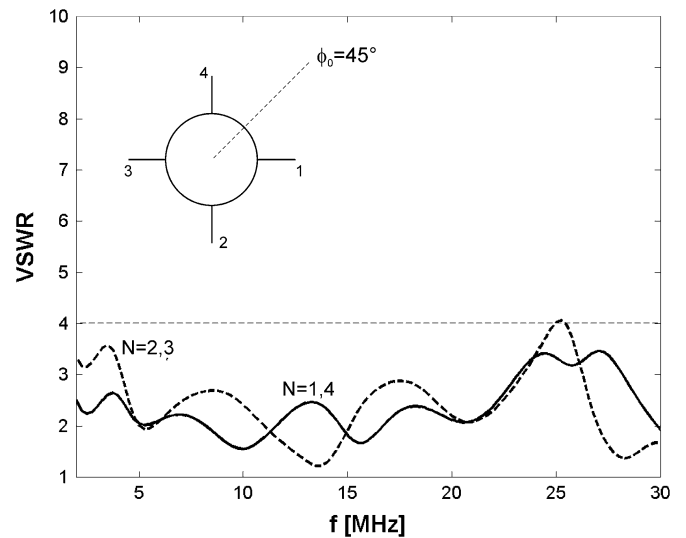


Fig. 16. VSWR of each source in NSA<sub>4</sub> when  $\phi_0 = 45^\circ$ ; due to the antenna rotational symmetry as regards  $\phi_0$ , pairs of symmetric sources share the same VSWR curve.

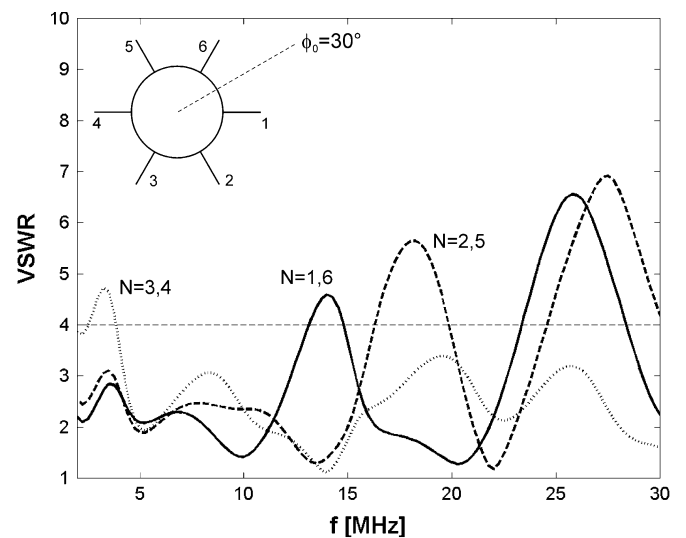


Fig. 17. VSWR of each source in NSA<sub>6</sub> when  $\phi_0 = 30^\circ$ ; due to antenna symmetry as regards  $\phi_0$ , pairs of symmetric sources share the same VSWR curve.

(Fig. 17). Hence, it can be necessary to compensate this behavior by introducing a proper matching network or by means of a more efficient array synthesis strategy, also accounting for matching requirements.

The choice  $\phi_0 = (m + 1/2)\Delta\phi$  permits to obtain symmetric patterns and to simultaneously minimize the mutual coupling among subradiators. In particular, the authors verified that antenna matching degrades as  $\phi_0$  moves from the central position between two adjacent subradiators toward one of them.

Finally, NSA<sub>N</sub> in monochannel configuration can be even used to emphasize the radiation toward the zenith for NVIS links in the range 2–7 MHz. By feeding a pair of opposite subradiators with equal signal amplitudes and opposite phases, the current on the antenna (Fig. 18) assumes the same distribution as on a large half-loop. Comparing the resulting 2 MHz pattern with that of the single-feed NSA (Fig. 6), it can be observed a gain

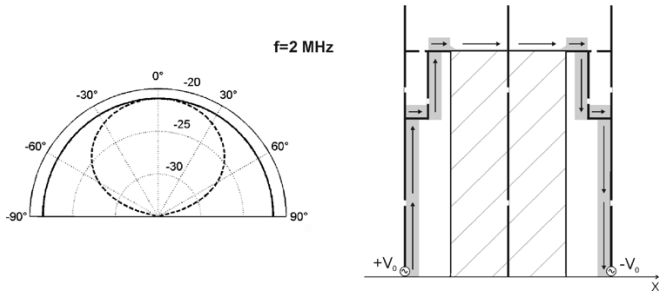


Fig. 18. Vertical gain pattern and current distribution on the NSA<sub>4</sub> at 2 MHz when a half-loop mode is excited; solid line:  $\phi = 0^\circ$ , dashed line:  $\phi = 90^\circ$ ; arrows indicate the current direction.

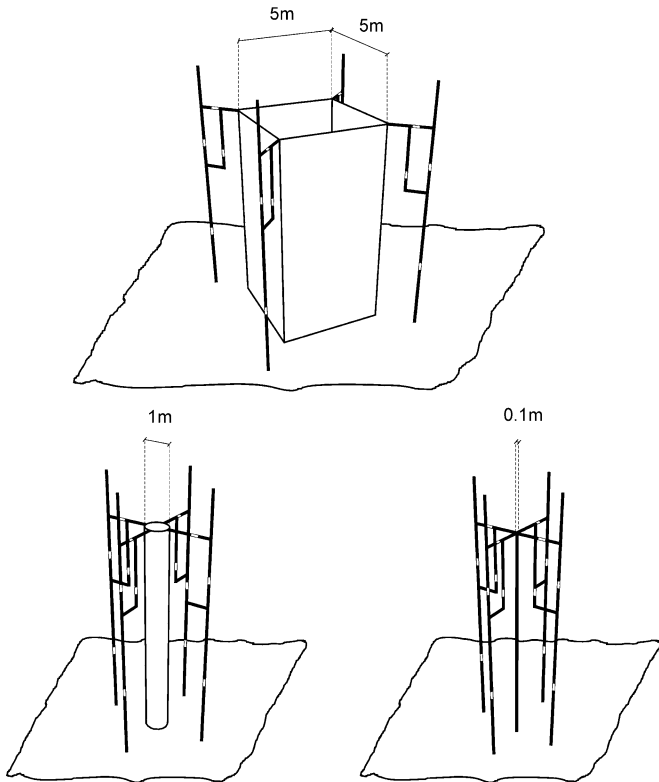


Fig. 19. Three alternative geometries for the multiport NSA system. The central conductor is a fat hollow square-size cylinder of 5 m side, a thin circular hollow cylinder of 1 m diameter, and a simple 0.1 m thickness wire. The wire subradiators are the same as in Fig. 3.

improvement of about 3–4 dB on the zenith and a more uniform radiation close to it. It has also been verified that the active subradiators still retain an acceptable matching ( $VSWR < 3.5$ ).

V. PERFORMANCES WITH DIFFERENT SUPERSTRUCTURES

The extension of the NSA<sub>N</sub> concept to different superstructures in order to better understand the role of the thickness and shape of the central conductor is investigated here. Three geometries have been considered (Fig. 19): a 5-m-square cross-section cylinder having wire subradiators in front of the wedges, a 1-m-diameter cylinder representative of a naval mast, and a simple wire that may yield a standalone general-purpose multiport broadband antenna system. Four ports are allocated (NSA<sub>4</sub>) in each configuration. Wire subradiators retain the

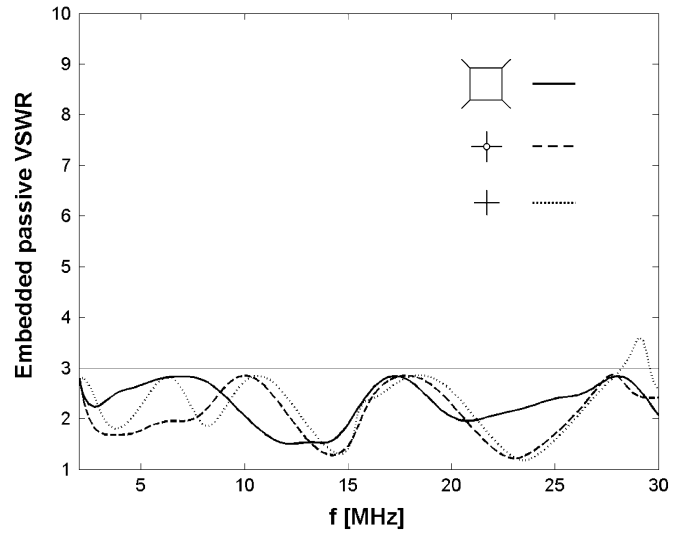


Fig. 20. Embedded VSZR of the three NSA<sub>4</sub> systems in Fig. 19 when the loading impedances have been reoptimized, according to the penalty function in (1) only for what concerns their values, while the topology and positions are the same as in Fig. 3.

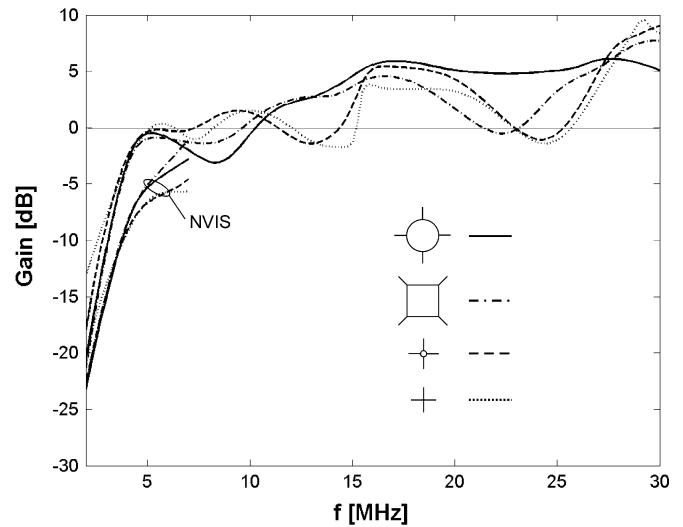


Fig. 21.  $\phi$ -averaged active gain of three NSA<sub>4</sub> systems in Fig. 19 after loading impedance reoptimization.

same shape as in the original NSA while the loading impedances are reoptimized, only for what concerns their values, having fixed the topology and positions as before. The multi-channel mode is checked, e.g., the active gain and efficiency and the embedded VSZR are calculated by means of the usual numerical models. It is expected, however, that even better results could be obtained with an ad hoc design of the wire subradiators.

In all the geometries the ports are well matched (Fig. 20) with VSZR well below 3:1 in most part of the HF band, quite apart from the size and shape of the central structure. The average active gains along the horizon (Fig. 21) reveal some differences, particularly at low frequencies (2–5 MHz). As the size of the central conductor is reduced, the active gain at the horizon increases since the structure acts more as a dipole rather than as an omnidirectional antenna, that is instead a feature of large central

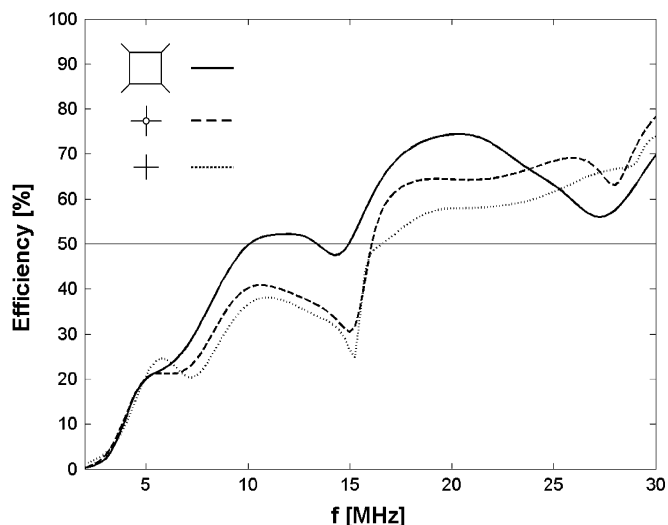


Fig. 22. System (active) efficiency of NSA<sub>4</sub> systems in Fig. 19 after loading impedance reoptimization. Curves have to be compared with the solid line in Fig. 10.

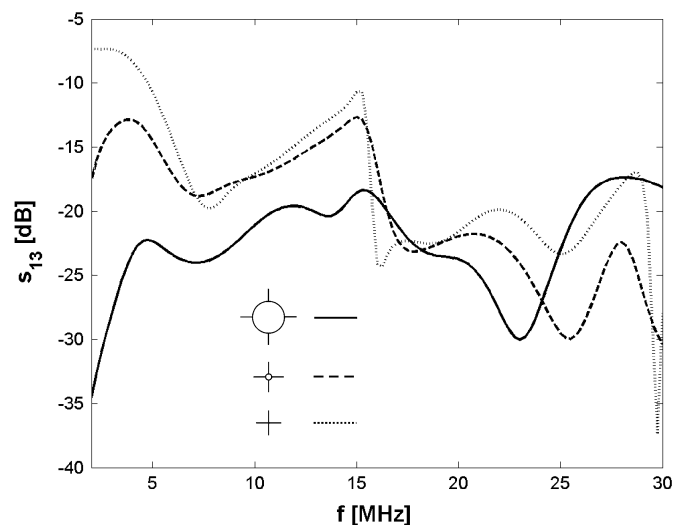


Fig. 23. Coupling parameters ( $S_{13}$ ) among antipodal ports for circular cylindrical NSAs with diameter 5, 1, and 0.1 m.

conductors. The thick circular- and square-section NSAs perform similarly, while systems with thinner central conductors exhibit a less uniform gain versus frequency.

More relevant differences in antenna performances appear in the active efficiency diagrams of Fig. 22, where the NSAs with a thinner central conductor are less efficient in most of the HF band. This effect is due to the overall reduced size of the antenna system and, hence, to a coupling among subradiators larger than that of the 5 m structure. For instance, as is visible in Fig. 23, the  $S_{13}$  scattering parameters between antipodal ports reveal a stronger interaction for thinner structures. In this case, part of the current injected by the active port in a subradiator will be both dissipated by the loading resistors of other subradiators and collected at the passive ports. The increase of interport coupling could also forbid the multichannel usage of the system with thin central conductors. When the same configurations are driven in monochannel mode (array), blind subbands (as in Fig. 17) are

visible, the efficiency is poor ( $<40\%$ ) in the whole HF band, and sectorial coverage is not possible at lower frequencies.

The authors also verified that even removing the central conductor, the resulting antenna system still retains the same features of NSA<sub>4</sub> equipped with a thin central conductor. The presence of a fat central structure seems therefore to be required to obtain high efficiency and a reasonable decoupling among ports rather than for broadbanding purposes.

## VI. CONCLUSION

This paper has theoretically verified the possibility of using a cylindrical naval superstructure, such as a funnel or a large mast, as an active part of an HF antenna system for both sea-wave and NVIS communications. The resulting structural antenna can be used as a single-feed and even as a multifeed radiator. When equipped with multiple ports and used in multichannel mode, NSA<sub>N</sub> permits highly improved system efficiency in comparison with a single broadband radiator equipped with a lossy combining network. A first benefit is a savings in the power supplied and a simplification of the cooling systems. When used in monochannel mode, instead, NSA<sub>N</sub> permits sectorial coverage with improvement in power handling. Additionally, due to its large size, the naval structural antenna could host other antenna types for higher frequencies (VHF/UHF) with the purpose of achieving a unique integrated antenna system for the whole Software Defined Radio band.

Finally, it has been verified that the multichannel multiport concept is applicable to support structures other than the fat cylinder, with efficiency mainly dependent on the size of the central structures, rather than on their shape. Nevertheless, those antenna systems with reduced size could be useful to stand-alone applications, different from the naval ones.

Further investigations will consider the experimental validation of the NSA concept by a scaled model and its implementation on naval platforms, where the real shape and size of the funnel or the big mast, and the surrounding environment, will be taken into account in an ad-hoc design procedure.

## ACKNOWLEDGMENT

The authors wish to thank M. Proia, G. Falcione, R. Perelli, and G. Colasanti for inspiration, M. Marrocco for technical support, and Prof. F. Bardati and Prof. P. Tognolatti for suggestions and valuable discussions.

## REFERENCES

- [1] E. Buracchini, "The software radio concept," *IEEE Commun. Mag.*, vol. 38, pp. 138–143, Sep. 2000.
- [2] J. V. N. Granger, "Shunt excited flat plate antennas with applications to aircraft structures," *Proc. IRE*, vol. 38, no. 3, pp. 280–287, Mar. 1950.
- [3] J. V. Tanner, "Shunt and notch-fed aircraft antennas," *IRE Trans. Antennas Propag.*, vol. 6, no. 1, pp. 35–43, Jan. 1958.
- [4] C. E. Baum, "Airframes as antennas," Air Force Research Lab. Sensor and Simulation Note 381, May 1995.
- [5] G. Marrocco and P. Tognolatti, "New method for modeling and design of multiconductor airborne antennas," *Proc. Inst. Elect. Eng. Microw. Antennas Propag.*, vol. 151, no. 3, pp. 181–186, Jun. 2004.
- [6] S. R. Best, "On the use of scale brass models in HF shipboard communication antenna design," *IEEE Antennas Propag. Mag.*, vol. 44, pp. 12–22, Apr. 2002.

- [7] M. Anstey and S. A. Saoudy, "Radiation characteristics of a ship-mounted high frequency ground wave radar antenna," in *Antennas Propag. Soc. Int. Symp.*, vol. 3, July 1996, pp. 1852–1855.
- [8] C. E. Baum, "Ship platform for HF/VHF arrays," Air Force Research Lab. Sensor and Simulation Note 383, Aug. 1995.
- [9] A. Boag, A. Boag, E. Michielssen, and R. Mittra, "Design of electrically loaded wire antennas using genetic algorithms," *IEEE Trans. Antennas Propag.*, vol. 44, pp. 687–695, May 1996.
- [10] G. J. Burke and A. J. Poggio, "Numerical electromagnetic code (NEC) method of moments, Pt. I and II," Naval Ocean Syst. Center, CA, Tech. Doc. 116, 1980.
- [11] L. Mattioni and G. Marrocco, "Design of a broad-band HF antenna for multi-mode naval communications," *IEEE Antennas Wireless Propag. Lett.*, vol. 4, pp. 179–182, 2005.
- [12] G. Marrocco, F. Bardati, M. Proia, P. Tognolatti, L. Mattioni, R. Perelli, G. Colasanti, and G. Falcione, "Multi-function broadband HF antenna for naval installation," Italian Patent TO2005A000 344 (pending).
- [13] Y. Rahmat-Samii and E. Michielssen, *Electromagnetic Optimization by Genetic Algorithms*. New York: Wiley, 1999, pp. 1–16.
- [14] Z. Altman, R. Mittra, and A. Boag, "New designs of ultra wide band communication antennas using a genetic algorithm," *IEEE Trans. Antennas Propag.*, vol. 45, pp. 1494–1501, Oct. 1997.
- [15] F. I. Tseng and D. K. Cheng, "Pattern synthesis of circular arrays with many directive elements," *IEEE Trans. Antennas Propag.*, vol. AP-16, p. 758, Nov. 1968.



**G. Marrocco** (M'98) received the Laurea degree in electronic engineering and the Ph.D. degree in applied electromagnetics from the University of L'Aquila, Italy, in 1994 and 1998, respectively.

Since 1997, he has been a Researcher at the University of Rome "Tor Vergata," Rome, Italy, where he currently teaches antenna design and bioelectromagnetics. In summer 1994, he was at the University of Illinois at Urbana-Champaign as Postgraduate Student. In autumn 1999, he was a Visiting Researcher at the Imperial College in London, London, U.K. He

has been involved in several space, avionic and naval programs of the European Space Agency, NATO, Italian Space Agency, and the Italian Navy. His research is mainly directed to the development of numerical methods and signal processing techniques for the time domain modeling and design of complex electromagnetic structures in the context of biological and aerospace applications.



**L. Mattioni** received the Laurea degree in telecommunications engineering from the University of Rome Tor Vergata, Italy, in 2004, where he is currently working toward the Ph.D. degree in electromagnetics.

In 2004, he was a Grant Researcher at the University of Rome Tor Vergata, working on broadband antennas for HF naval communications. His scientific interests are the modeling and design of innovative broadband antenna systems for mobile platforms and for the Software Defined Radio technology.